Available online at www.sciencedirect.com
SCIENCE DIRECT®
Biomaterials 25 (2004) 5323–5331
Biomaterials
www.elsevier.com/locate/biomaterials

The effect of pH on the structural evolution of accelerated biomimetic apatite

Yu-Fen Chou[a], Wen-An Chiou[b], Yuhuan Xu[c], James C.Y. Dunn[a,d], Benjamin M. Wu[a,c,e,*]

[a] Department of Bioengineering, UCLA, 7523 Boelter Hall, Los Angeles, CA 90095, USA
[b] Department of Chemical Engineering and Materials Science, UCI, 636E Engineering Tower, Irvine, CA 92697, USA
[c] Department of Materials Science and Engineering, UCLA, 6531 Boelter Hall, Los Angeles, CA 90095, USA
[d] Department of Surgery, UCLA, CHS 72-172, Los Angeles, CA 90095, USA
[e] Weintraub Center for Reconstructive Biotechnology, UCLA, CHS B3-068, Los Angeles, CA 90095, USA

Received 17 October 2003; accepted 10 December 2003

Abstract

The classic biomimetic apatite coating process can be accelerated by first immersing substrates into concentrated simulated body fluid, 5× SBF (SBF1), at 37°C, to form an initial coating of precursor apatite spheres, and subsequently transferring to a second 5× SBF (SBF2) solution which is devoid of crystal growth inhibitors to promote phase transformation of SBF1-derived precursor apatite spheres into final crystalline apatite plates. Since SBF1 governs the formation kinetics and composition of the initial precursor spheres, we hypothesized that the pH of the SBF1 solution will also influence the final structure of the SBF2-derived crystalline apatite. To test this hypothesis, polystyrene substrates were immersed into SBF1 with different pH (5.8 or 6.5), and then immersed into the identical SBF2 (pH = 6.0). The resultant apatites exhibited similar 2θ XRD peaks; FTIR spectra in terms of hydroxyl, phosphate and carbonate groups; and Ca/P atomic ratio (1.42 for $SBF1_{5.8}$ apatite; 1.48 for $SBF1_{6.5}$ apatite). SEM, TEM and electron diffraction show that while $SBF1_{6.5}$ (pH 6.5) precursor spheres transform into larger, single crystals plates, $SBF1_{5.8}$ (pH 5.8) precursor spheres developed minute, polycrystalline plate-like structures over predominantly spherical precursor substrate.

Keywords: Apatite Structure; Bone tissue engineering; Biomimetic material; Simulated body fluid

1. Introduction

Formation of a carbonated apatite layer has been shown to be an important phenomenon leading to direct bone bonding onto bioactive ceramic surfaces in vivo [1]. Kokubo et al. demonstrated systematically that a material's in vivo bioactivity could be directly related to the rate at which the material forms apatite in vitro when immersed in simulated body fluids (SBF) [2–5]. The so-called biomimetic apatite coating technique [6] has been employed by numerous investigators to produce apatite coating over implant surfaces [7,8] and within three-dimensional degradable scaffolds [9]. Besides reducing fibrous encapsulation layer [10] and promoting direct bone contact [11], these biomimetic apatites have also been shown to promote differentiation of bone marrow stromal cells along osteogenic lineage [12].

Recently, Barrere et al. [13,14] accelerated the classical biomimetic process from 7 to 14 days to 1 day by immersing substrates into supersaturated SBF (5× SBF), and illustrated systematically the interdependence of ionic strength, pH, carbonate concentration, and their collective influence on the formation of the resultant apatite. It has been known for some time that solution pH affects apatite formation kinetics in the 1.5× SBF, which occurs at pH 7.0. Low solution pH is required to increase ionic solubility that is necessary for the supersaturated SBFs if the accelerated techniques were applied. Also, pH was indirectly controlled by ionic strength and carbonate concentration of SBF solutions. However, on the mineralization process, the effect of pH on apatite structure is not known.

We recently described the detailed structural evolution of apatite under a similar accelerated process [15],

*Corresponding author. Department of Bioengineering, UCLA, 7523 Boelter Hall, Los Angeles, CA 90095, USA. Tel.: +1-310-794-7094.
E-mail address: benwu@ucla.edu (B.M. Wu).

0142-9612/$ - see front matter © 2004 Elsevier Ltd. All rights reserved.
doi:10.1016/j.biomaterials.2003.12.037

where substrates were immersed into concentrated simulated body fluid, 5× SBF (SBF1), at 37°C, and subsequently transferred to a second 5× SBF (SBF2) solution which is devoid of Mg^{2+} and HCO_3^-. In supersaturated SBF1, aqueous ions nucleate to form atomic calcium phosphate clusters, which further aggregate to form amorphous calcium phosphate (ACP) precursor spheres. Ab initio calculations of the $Ca_3(PO_4)_2$ cluster potential energy surface suggest the trimeric Posner's cluster $[Ca_3(PO_4)_2]_3$ as the most stable configuration for ACP, but several isomers may co-exist [16]. The precursor spheres may attach onto the biomaterial surfaces, or continue to grow in solution, until they gain enough mass and fall in solution. In SBF2, the absence of crystal growth inhibitors facilitates the phase transformation of SBF1-derived precursor apatite spheres into crystalline apatite plates. Although the precise mechanism of this transformation is unknown, it is noteworthy that Ca and PO_4 occupy nearly identical atomic positions in $[Ca_3(PO_4)_2]_3$, ACP, and apatite structures. Since pH may influence the kinetics of $Ca_3(PO_4)_2$ cluster formation/dissolution, and the composition of the initial precursor spheres, the purpose of this study is to investigate the influence of solution pH of initial SBF1 on microstructural evolution and final apatite structure.

2. Materials and methods

2.1. Materials preparation

2.1.1. 5× simulated body fluid (SBF) preparation

All reagents were purchased from EM science. 5× SBF was prepared by sequentially dissolving $CaCl_2$, $MgCl_2 \cdot 6H_2O$, $NaHCO_3$, and $K_2HPO_4 \cdot 3H_2O$ in distilled deionized water. Solution pH was lowered to 6 by adding concentrate HCl to increase the solubility. Na_2SO_4, KCl and NaCl were added until the previous solution become clear. The final pH was adjusted with 1 M sodium hydroxide or 1 M hydrochloric acid to have final pH equaled to 5.8 ($SBF1_{5.8}$) or 6.5 ($SBF1_{6.5}$).

Mg^{2+} and HCO_3^- free 5× SBF (SBF2) was prepared by adding NaCl, $CaCl_2$, and $K_2HPO_4 \cdot 3H_2O$ subsequently to distilled deionized water. Solution pH was lowered to 6.0 with hydrochloric acid to increase the solubility.

All solutions were sterile filtered through 0.22 μm PES membrane (Nalgene, NY). Table 1 lists the ionic concentration of blood plasma, 5× SBF (SBF1) and Mg^{2+} and HCO_3^- free 5× SBF (SBF2) (Concentrations of SBF1 and SBF2 were obtained from calculation). All solutions were prepared freshly before usage.

Table 1
The ionic concentration of human blood plasma, SBF1 and SBF2

Ion conc. (mM)	Na^+	K^+	Ca^{2+}	Mg^{2+}	HCO_3^-	Cl^-	HPO_4^{2-}	SO_4^{2-}
Blood plasma	142	5	2.5	1.5	27	103	1	0.5
SBF1	710	25	12.5	7.5	21	740	5	2.5
SBF2	710	10	12.5	0	0	735	5	0

2.1.2. Biomimetic process

Accelerated biomimetic apatite coatings were prepared in two different conditions.

Low pH SBF1 (pH = 5.8; $SBF1_{5.8}$): Non-treated polystyrene culture dishes (Corning# 430588, PA) were argon plasma etched (Harrick Scientific, NY) following by incubating in 5× SBF (simulated body fluid) (pH 5.8) for 1 day, and changed to Mg^{2+} and HCO_3^- free 5× SBF (pH 6.0; SBF2) for another 2 days. The solution temperature was controlled at 37°C.

High pH SBF1 (pH = 6.5; $SBF1_{6.5}$): All steps were the same with low pH except that the initial pH of 5× SBF1 was 6.5. The same Mg^{2+} and HCO_3^- free SBF2 were used (pH 6.0).

After 1 day immersion in SBF1 and 2 days immersion in SBF2, all substrate surfaces were gently rinsed with sterile ddH_2O to remove excess ions and dried in a laminar flow hood prior to characterization.

2.2. Materials characterization

2.2.1. Electron microscopy

The apatite coated polystyrene dishes were cut to the SEM stub size. The specimens were then coated with a thin layer of carbon to improve the conductivity. The biomimetic apatite was observed with a field emission SEM (Phillips/FEI XL-30) that equipped with EDX (energy-dispersive spectrometer) for microchemical analysis. For TEM observation, the apatite was scraped gently from the surface of substrate, and re-suspended in isopropanol. One or 2 drops of the suspension were pipetted onto a Holey carbon grid and observed in a TEM (Phillips/FEI CM-20). While low magnification images were taken to analyze the apatite morphology, high-resolution TEM and electron diffraction were applied to obtain lattice images and diffraction patterns for crystallographic study, respectively.

2.2.2. XRD analysis

XRD spectra were obtained using Siemens D5000 X-ray diffractometer (CuKα radiation, 40 kV and 30 mA). Data were collected in the range of $2\theta = 20$–60° using 0.05° step and 3 s/step scan speed.

2.2.3. Attenuated total reflection-Fourier transform infrared spectroscopy (ATR-FTIR)

Apatite powders were gently scraped from substrate, and placed in contact with diamond ATR window. FTIR (Avatar 360 Thermo Nicolet spectrometer) transmittance spectra from 4000 to 500 cm^{-1} wavenumbers were obtained.

3. Results and discussions

3.1. Apatite precursor spheres formation after 24 h in SBF1

After 1 day immersion in $SBF1_{6.5}$, the solution became cloudy and a layer of opaque coating deposited onto the dish. On the contrary, the $SBF1_{5.8}$ solution remained clear during immersion (Fig. 1). Smooth spheres were observed in both high and low pH conditions in the SEM. The size ranges from 100 nm to 1.5 μm. The higher opaqueness of $SBF1_{6.5}$-treated substrates as compared with $SBF1_{5.8}$-treated substrates after 1 day of immersion is probably due to the enhanced solution precipitation at higher pH. EDX confirms the presence of calcium and phosphorus with the Ca/P atomic ratio around 1.27 (Fig. 2, data from high pH sample). FTIR spectrum reveals the precursor spheres contain OH, PO_4^{3-} and CO_3^{2-} functional groups (Fig. 3). Although precursor spheres from $SBF1_{6.5}$ and $SBF1_{5.8}$ exhibit similar spherical morphology and calcium/phosphorus content, it is not known if the precursor spheres were comprised of different $[Ca_3(PO_4)_2]_n$ cluster arrangements. We hypothesize that

Fig. 1. One day immersion in SBF1. Top two rows were immersed in high initial pH ($SBF1_{6.5}$), and the solution looks more opaque. Bottom two rows were immersed in low initial pH ($SBF1_{5.8}$), and the solution remains clear.

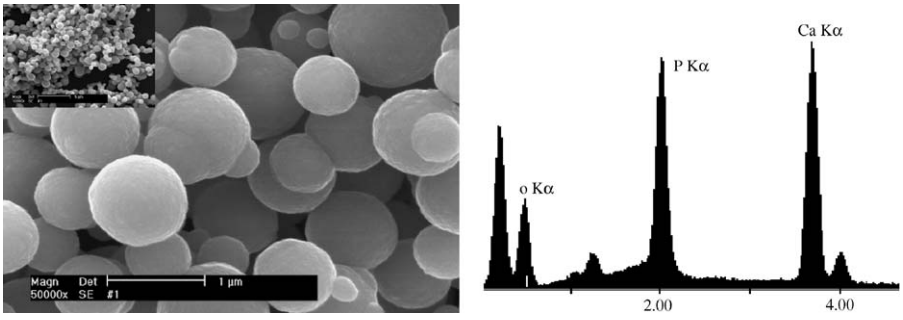

Fig. 2. After 1 day immersion in $SBF1_{6.5}$, the precursor smooth spheres have formed on top of the polystyrene dish. The sphere sizes range from 100 nm to 1.5 μm. EDX confirms the presence of calcium and phosphorus, and the Ca/P $\sim$1.27.

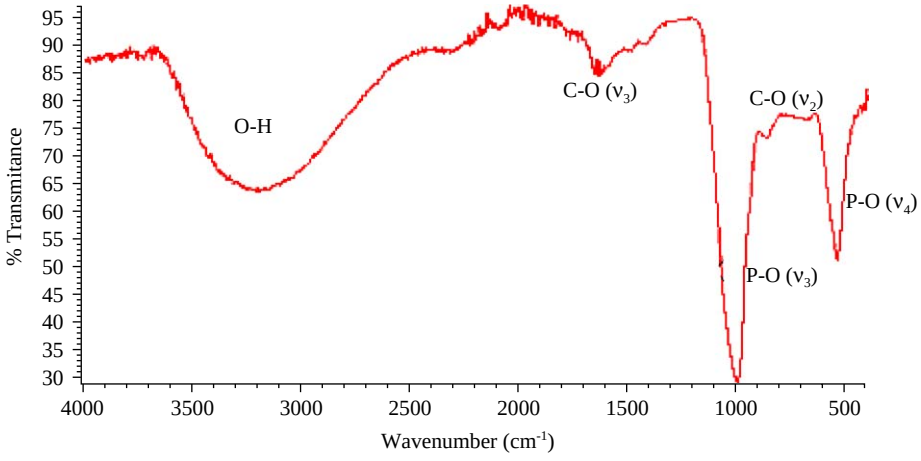

Fig. 3. After 1 day immersion in high pH SBF1, the FTIR spectrum shows broad band for −OH, and reveals the presence of PO_4^{3-} and CO_3^{2-} functional groups.

higher initial pH promotes precipitation of more precursor spheres which are comprised of fewer stable and more unstable cluster arrangements which will subsequently undergo rapid phase transformation into plate-like structures while immersion in SBF2.

3.2. Apatite crystalline plates formation after 1 day in SBF1 and 2 days in SBF2

After 1 day immersion in SBF1 and 2 days in SBF2, all precursor spheres from both high and low pH conditions were transformed into plate-like morphology (Fig. 4). Although identical SBF2 was used as the second solution for both SBF1 (pH = 5.8 vs. 6.5) solutions, it was obvious to the naked eye that substrates that were initially immersed in $SBF1_{6.5}$ appeared more opaque when compared to the substrates immersed initially in $SBF1_{5.8}$. The result was similar to that 1 day of immersion in SBF1, so that $SBF1_{6.5}$ samples still remained more opaque. The SEM images (Fig. 4) demonstrated clear morphological difference in their plate-like apatite structure. Relative to $SBF1_{5.8}$, the high initial pH condition ($SBF1_{6.5}$) contributes to much larger plate-like structure formation (Figs. 4a–c). The plates from $SBF1_{6.5}$ (thickness ranges from 40 to 100 nm, and the length ranges from 1 and 5 μm) were significantly larger than the plates from $SBF1_{5.8}$ (Figs. 4(d, e and f)). EDX in Figs. 4a and d showed that both apatites contain primarily Ca and P, and with Ca/P ratio below the stoichiometric 1.67 for hydroxyapatite [$Ca_{10}(PO_4)_6(OH)_2$]. The Ca/P ratio of $SBF1_{6.5}$ is 1.48 slightly higher than that of $SBF1_{5.8}$ (= 1.42). The formation of calcium deficient apatites may involve cation substitutions at the Ca^{2+} sites, and/or the substitution at PO_4^{3-} sites by HPO_4^{2-} ions, with the concomitant creation of calcium vacancies in order to satisfy the condition of electrical charge neutrality.

ATR-FTIR spectra (Fig. 5) of high and low pH apatites exhibit broad bands for O–H stretching $\sim 3400\,cm^{-1}$; sharp peaks for PO_4^{3-}: $1043\,cm^{-1}$ (v_3), $960\,cm^{-1}$ (v_1) and $560\,cm^{-1}$ (v_4); and also for CO_3^{2-}: $1500\,cm^{-1}$ (v_3), and $870\,cm^{-1}$ (v_2). Both apatites exhibited similar FTIR spectra which match that for hydroxyapatite except for the presence of CO_3^{2-} groups.

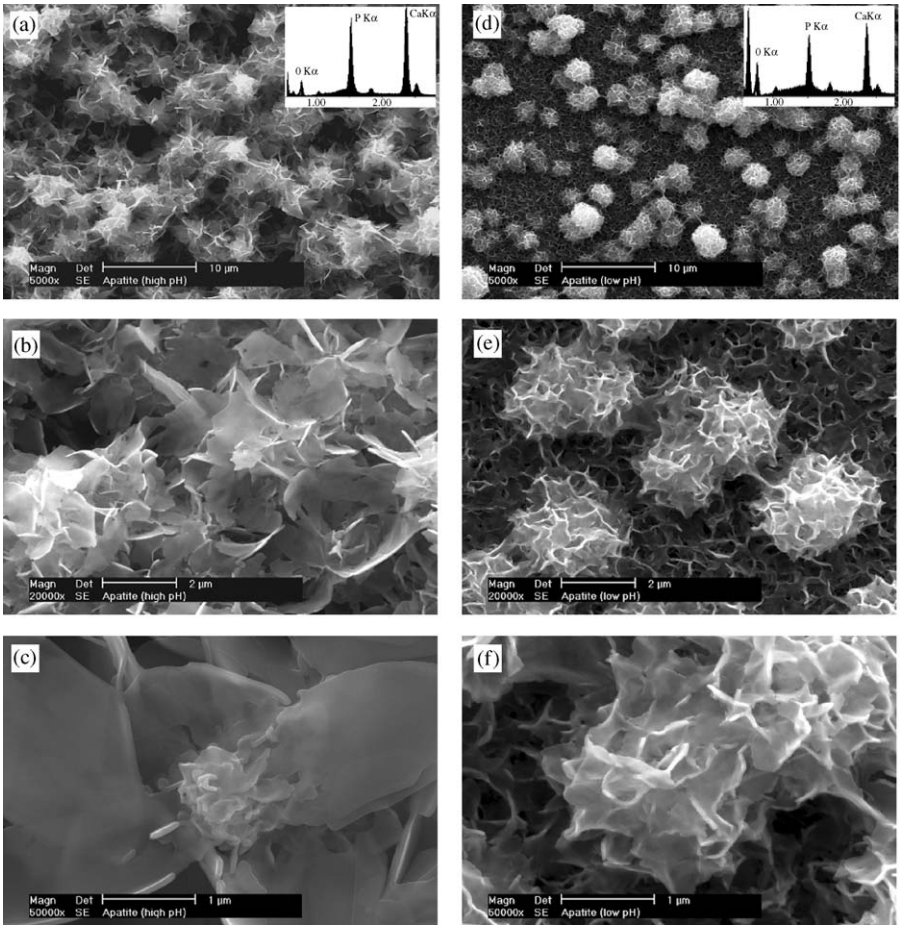

Fig. 4. SEM observation of the biomimetic apatite after 1 day immersion in SBF1 and 2 days immersion in SBF2. (a, b and c) High initial pH ($SBF1_{6.5}$) represents larger plate-like structure. (d, e and f) Low initial pH ($SBF1_{5.8}$) represents smaller plate-like structure. (a) EDX confirms the calcium and phosphorus content (Ca/P ~1.48) for the high initial pH apatite. (d) EDX confirms the calcium and phosphorus content (Ca/P ~1.42) for the low initial pH apatite.

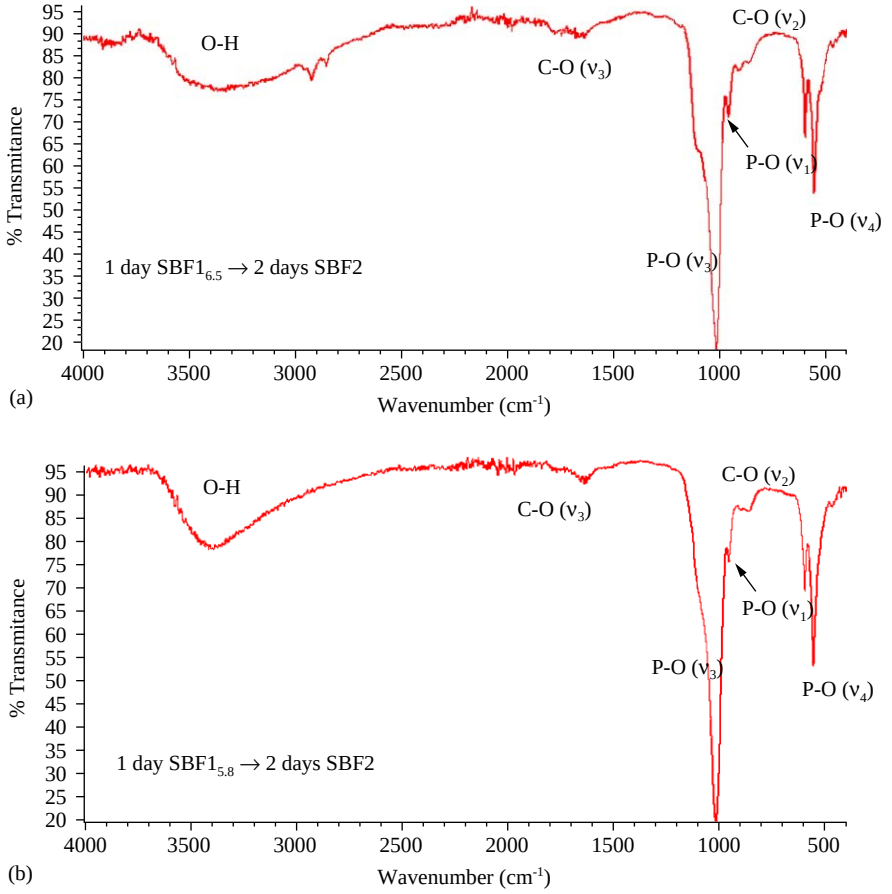

Fig. 5. ATR-FTIR spectra of the biomimetic apatite after 1 day immersion in SBF1, and 2 days in SBF2. (a) High initial pH (b) Low initial pH. Both of the spectra reveal −OH, phosphate and carbonate functional groups. Both FTIR spectra exhibit broad bands for O–H stretching $\sim 3400\,cm^{-1}$; sharp peaks for PO_4^{3-}: $1043\,cm^{-1}$ (v_3), $960\,cm^{-1}$ (v_1) and $560\,cm^{-1}$ (v_4); and also for CO_3^{2-}: $1500\,cm^{-1}$ (v_3), and $870\,cm^{-1}$ (v_2). The CO_3^{2-} functional groups suggest carbonate ions are incorporated in the biomimetic apatite and form carbonate-hydroxyapatite $[Ca_{10}(PO_4)_3(CO_3)_3(OH)_2]$.

The presence of CO_3^{2-} functional groups suggests that carbonate ions are incorporated in the biomimetic apatite and form carbonate-hydroxyapatite $[Ca_{10}(PO_4)_3(CO_3)_3(OH)_2]$. Besides the bicarbonate ions in the SBF1 solutions, the CO_2 from the ambient air would also dissolve in the solution during this process. Under these conditions, it is less likely for carbonate-free hydroxyapatites to form.

The XRD spectra are shown in Fig. 6, and the major and minor peaks are listed in Tables 2 and 3. The two apatites also exhibited similar XRD spectra with major peaks at $d = 2.81$, 2.72 and 3.44 Å corresponding to (2 1 1), (1 1 2) and (0 0 2) planes of hydroxyapatite $[Ca_{10}(PO_4)_6(OH)_2]$, respectively, except the intensity was slightly higher in $2\theta = 32.2°$ in low initial pH sample (Fig. 6b). The minor component is likely carbonate-hydroxyapatite $[Ca_{10}(PO_4)_3(CO_3)_3(OH)_2]$ due to similar d spacings ($2\theta = 32.17°$, 33.4° and 25.76°) which could be overlapped with hydroxyapatite (JCPDS Standard for hydroxyapatite 9-432 and carbonate-hydroxyapatite 9-272).

TEM observation, however, shows that final apatites formed from high and low pH SBF1 solutions are quite different morphologically. Apatite formed in SBF1$_{6.5}$ exhibited large plate-like structure. TEM micrograph (Fig. 7a) clearly shows an apatite plate from SBF1$_{6.5}$. While photographing higher magnification TEM images, small circular features began to form within 10 s on the surface of SBF1$_{6.5}$ apatite platelets (Figs. 7b and c) due to irradiation damage from electron beam. These irradiation defects continued to change dynamically, as the circular features enlarged and merged with each other. On the other hand, this irradiation phenomenon was not observed with the apatite plates formed from low pH SBF1$_{5.8}$. This observation suggests the apatite from SBF1$_{6.5}$ (high pH) is more unstable against irradiation, and the instability may be due to the presence of more soluble phases in the precursor spheres formed after 1 day immersion in SBF1$_{6.5}$ (high pH). This observation is also consistent with our hypothesis that higher initial pH promotes faster precipitation of precursor spheres which are comprised of fewer stable, and more unstable phases which will subsequently undergo rapid phase transformation into large plate-like structures which remain relatively unstable under electron beam. SBF1$_{6.5}$ (high pH) forms single crystal

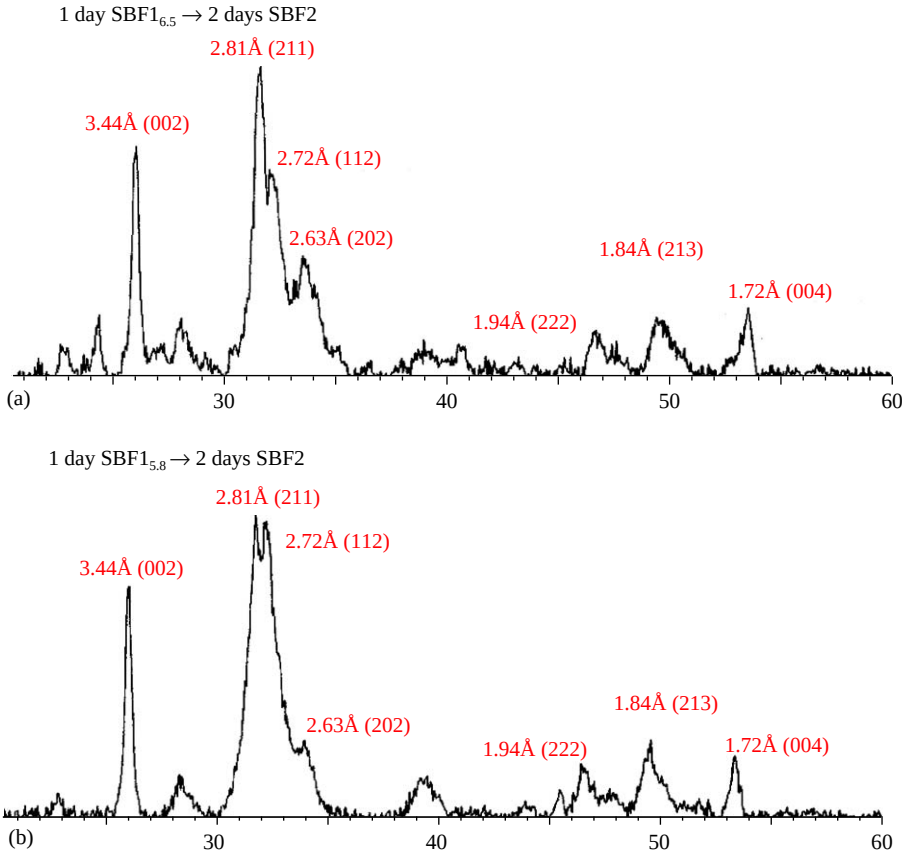

Fig. 6. XRD spectra of the biomimetic apatite after 1 day immersion in SBF1, and 2 days in SBF2. (a) High initial pH (b) Low initial pH. The two apatites exhibited similar XRD spectra with major peaks at $d = 3.44$, 2.81 and 2.72 Å corresponding to (2 1 1), (1 1 2) and (0 0 2) planes of hydroxyapatite [$Ca_{10}(PO_4)_6(OH)_2$], respectively. The minor component could be carbonate-hydroxyapatite [$Ca_{10}(PO_4)_3(CO_3)_3(OH)_2$] due to similar d spacings ($2\theta = 32.17°$, 33.4° and 25.76°) which could be overlapped with hydroxyapatite (JCPDS Standard for hydroxyapatite 9-432 and carbonate-hydroxyapatite 9-272).

Table 2
Major peaks in the XRD spectra of the accelerated biomimetic apatite which match with hydroxyapatite (JCPDS Standard 9-432 [$Ca_{10}(PO_4)_6(OH)_2$])

d space (Å)	2θ	($h\,k\,l$)	Intensity
3.44	25.879°	(0 0 2)	40
2.81	31.773°	(2 1 1)	100
2.72	32.196°	(1 1 2)	60
2.63	34.040°	(2 0 2)	25
1.94	46.711°	(2 2 2)	30
1.84	49.468°	(2 1 3)	40
1.72	53.143°	(0 0 4)	20

Table 3
Minor peaks in the XRD spectra of the accelerated biomimetic apatite which match with carbonate-hydroxyapatite (JCPDS Standard 9-272 for [$Ca_{10}(PO_4)_3(CO_3)_3(OH)_2$])

d space (Å)	2θ	($h\,k\,l$)	Intensity
3.46	25.726°	(0 0 2)	25
2.78	32.172°	(1 1 2)	100
2.68	33.407°	(3 0 0)	40

apatites as shown by electron diffraction pattern in Fig. 7(b). Three electron spots which were the brightest and closest to the incident beam were calculated, and revealed $d_1 = 2.81$ Å, $d_2 = 3.44$ Å and $d_3 = 2.72$ Å. The result corresponds to the major three peaks (Fig. 6a; $2\theta = 31.7°$, 25.9° and 32.2°) in XRD. The lattice fringes of a SBF1$_{6.5}$ apatite plate are clearly depicted by high-resolution TEM (Fig. 7c).

Conversely, apatite morphology of low initial pH condition (SBF1$_{5.8}$) shows somewhat thicker and more opaque image as compared with the large platelets formed in high initial pH condition. The surface of small platelets was not smooth, and revealed somewhat rough topography (Figs. 8a and c). In some areas, the needle-like structures were observed, and may correspond to longitudinal orientation of the small platy apatite (Fig. 8b). Fig. 8c shows a close-up view of the rough surface on small apatite platelet, and the electron diffraction pattern revealed the polycrystalline structure. High-resolution TEM image depicts the lattice fringes of biomimetic apatite grown in the low initial pH (Fig. 8d).

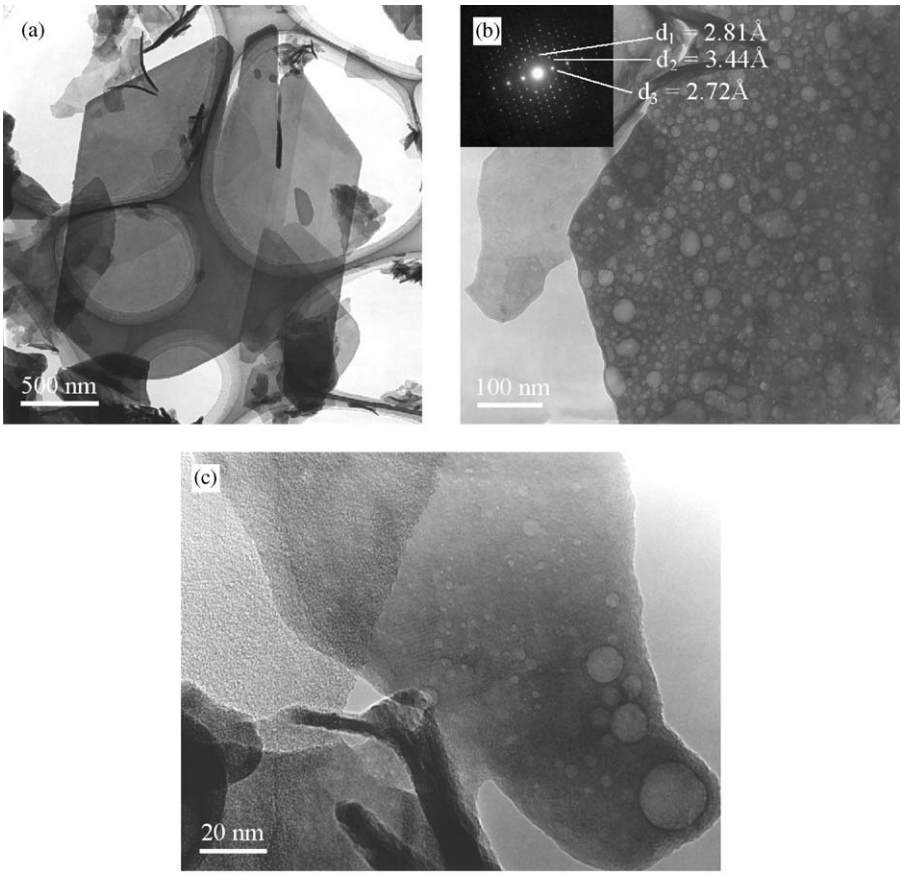

Fig. 7. TEM images obtained from the biomimetic apatite immersed in $SBF1_{6.5}$ (High pH) for 1 day, and changed to SBF2 for 2 days. (a) TEM bright field image clearly depicts the large, plate-like morphology. (b) Higher magnification image was taken from image a. During TEM observation, circular features appeared on the apatite plate's surface. (within 10 s). High-energy electron beam may cause the unstability of apatite plates. The electron diffraction pattern was taken from the edge of the apatite plate, and presented the single crystal structure. Three electron spots which were the brightest and closest to the incident beam were calculated, and revealed $d_1 = 2.81$ Å, $d_2 = 3.44$ Å and $d_3 = 2.72$ Å which correspond to (2 1 1), (0 0 2) and (1 1 2) planes of hydroxyapatite. (c) High-resolution TEM image depicts the lattice fringes of the plate-like biomimetic apatite.

SBF1 and SBF2 were freshly prepared in this study. This is important since the pH of SBF solutions can increase during storage. Within 1 week of storage at 4°C, the pH of $SBF1_{5.8}$ increased from 5.8 to 6.7, even though the solution remained clear (unpublished observation). In contrast, the pH of SBF2 remained relatively stable during storage at 4°C. When polystyrene was immersed in aged $SBF1_{5.8}$ solution (pH 6.7) for 1 day, and then changed to fresh SBF2 for 2 days, the resultant of large plate-like apatites resembled to those obtained from fresh $SBF1_{6.5}$ (data not shown). Therefore, it is critical to monitor the pH of the initial SBF1 solution since initial pH can result in distinctive apatite morphology.

Jianguo [17] reported that different pH buffering capacities of the regular 1 × SBF affected Ca/P molar ratios and chemical compositions of the precipitates at 37°C for one month. In contrast, this report described the effect of different initial pH of SBF1 causing morphological difference in the accelerated biomimetic apatite in 3 days.

It is not known whether the difference in surface texture and surface roughness is significant or not in terms of biological response [18], such as proliferation and spreading. Microtexturing by ion beam lithography was recently shown to improve osteoblast adhesion on polymer substrates, presumably due to the roughened surface as well as the implanted ions [19]. Micro- [20] and nano- [21,22] topography has also been shown to alter cellular morphology, cytoskeleton and proliferation. Besides topography, pH may also influence surface chemistry. Although the results reveal similar chemical structure (hydroxyl, phosphate and carbonate groups) in FTIR spectra, similar Ca/P atomic ratio (1.48 vs. 1.42), and similar 2θ major peaks, the TEM electron diffraction patterns demonstrated single crystal structure in larger plate-like particles (high pH) relative to the polycrystalline structure in the low pH apatite. Although this paper shows that initial pH of SBF1 solution controls final apatite plate morphology and chemical stability, the effect of these parameters on biological performance is unknown.

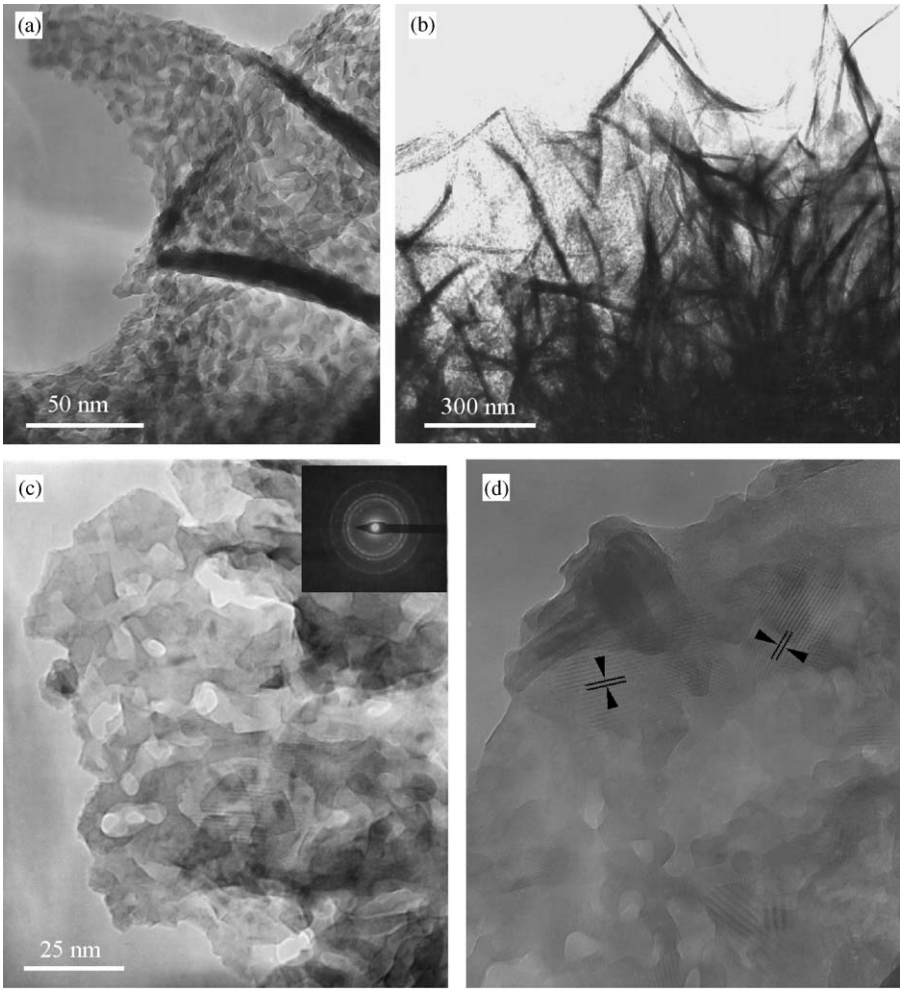

Fig. 8. TEM images obtained from the biomimetic apatite formed in $SBF1_{5.8}$ (Low pH) for 1 day, and changed to SBF2 for 2 days. (a) Low magnification TEM image shows the small plate-like structure. The surface is rough and contains lots of small budding structures. (b) Numerous thin, needle-like projections were observed. These features may be longitudinal orientation of plates with respect to the TEM thin section. (c) A close-up view of the apatite. The electron diffraction pattern reveals the polycrystal structure in nature. (d) High-resolution TEM image shows the lattice fringes (arrows) of biomimetic apatite.

4. Conclusion

Accelerated biomimetic apatite coating process can be achieved by first immersing substrates into concentrated simulated body fluid, $5\times$ SBF (SBF1), at 37°C, to form an initial coating of precursor apatite spheres, and subsequently transferring to a second $5\times$ SBF (SBF2) solution which is devoid of crystal growth inhibitors to promote phase transformation of SBF1-derived precursor apatite spheres into final crystalline apatite plates. Since SBF1 governs the formation kinetics and composition of the initial precursor spheres, this study showed that the pH of the SBF1 solution also influenced the final structure of the SBF2-derived crystalline apatite. SEM, TEM, and electron diffraction showed that while $SBF1_{6.5}$ precursor spheres transformed into larger, single crystals plates, $SBF1_{5.8}$ precursor spheres developed minute, polycrystalline plate-like structures over predominantly spherical precursor substrate.

Acknowledgements

This research was sponsored by NIH/NIDCR (1RO3 DE12956-01A).

References

[1] Hench LL. Bioceramics—from concept to clinic. J Am Ceram Soc 1991;74(7):1487–510.
[2] Tanahashi M, Yao T, Kokubo T, Minoda M, Miyamoto T, Nakamura T, Yamamuro T. Apatite coating on organic polymers by a biomimetic process. J Am Ceram Soc 1994;77(11):2805–8.
[3] Tanahashi M, Yao T, Kokubo T, Minoda M, Miyamoto T, Nakamura T, Yamamuro T. Apatite coated on organic polymers by biomimetic process: improvement in its adhesion to substrate by glow-discharge treatment. J Biomed Mater Res 1995;29:349–57.
[4] Miyaji F, Kim HM, Handa S, Kokubo T, Nakamura T. Bonelike apatite coating on organic polymers: novel nucleation process using sodium silicate solution. Biomaterials 1999;20:913–9.

[5] Fujibayashi S, Neo M, Kim HM, Kokubo T, Nakamura T. A comparative study between in vivo bone ingrowth and in vitro apatite formation on Na_2O–CaO–SiO_2 glasses. Biomaterials 2003;24(8):1349–56.
[6] Kokubo T, Kushitani H, Sakka S, Kitsugi T, Yamamuro T. Solutions able to reproduce in vivo surface-structure changes in bioactive glass-ceramic A-W3. J Biomed Mater Res 1990;24(6):721–34.
[7] Li P. Biomimetic nano-apatite coating capable of promoting bone ingrowth. J Biomed Mater Res 2003;66A(1):79–85.
[8] Nagano M, Kitsugi T, Nakamura T, Kokubo T, Tanahashi M. Bone bonding ability of an apatite-coated polymer produced using a biomimetic method: a mechanical and histological study in vivo. J Biomed Mater Res 1996;31:487–94.
[9] Zhang R, Ma PX. Porous poly(L-lactic acid)/apatite composites created by biomimetic process. J Biomed Mater Res 1999;45(4):285–93.
[10] Nagano M, Kitsugi T, Nakamura T, Kokubo T, Tanahashi M. Bone bonding ability of an apatite-coated polymer produced using a biomimetic method: a mechanical and histological study in vivo. J Biomed Mater Res 1996;31(4):487–94.
[11] Yan WQ, Nakamura T, Kawanabe K, Nishigochi S, Oka M, Kokubo T. Apatite layer-coated titanium for use as bone bonding implants. Biomaterials 1997;18(17):1185–90.
[12] Ohgushi H, Caplan AI. Stem cell technology and bioceramics: from cell to gene engineering. J Biomed Mater Res 1999;48(6):913–27.
[13] Barrere F, Blitterswijk CA, Groot K, Layrolle P. Influence of ionic strength and carbonate on the Ca–P coating formation from SBF × 5 solution. Biomaterials 2002;23(9):1921–30.
[14] Barrere F, Blitterswijk CA, Groot K, Layrolle P. Nucleation of biomimetic Ca–P coatings on Ti6Al4 V from a SBF × 5 solution: influence of magnesium. Biomaterials 2002;23(10):2211–20.
[15] Wulur IH. Microstructural control of biomimetically grown bonelike minerals on two dimensional and three dimensional polymer surfaces. M.S. thesis, Dept. of Bioengineering, UCLA, 2002.
[16] Gabin T, Pierre L, Noriko K, Kazuo O, Atsuo I. Existence of Posner's cluster in vacuum. J Phys Chem A 2000;104(21):5111–4.
[17] Jianguo L, Hailhong L, Malena S. Characterization of calcium phosphates precipitated from simulated body fluid of different buffering capacities. Biomaterials 1997;18:743–7.
[18] Wei H, Kenneth EG, Nikola B, Dave BP, Emily A, Michael H. Micro/nanomachining of polymer surface for promoting osteoblast cell adhesion. Biomed Microdevices 2003;5(2):101–8.
[19] Duncan AC, Weisbuch F, Rouais F, Lazare S, Baquey C. Laser microfabricated model surfaces for controlled cell growth. Biosensors Bioelectronics 2002;17:413–26.
[20] Linez-Bataillon P, Monchau F, Bigerelle M, Hildebrand HF. In vitro MC3T3 osteoblast adhesion with respect to surface roughness of Ti6Al4 V substrates. Biomol Eng 2002;19:133–41.
[21] Dalby MJ, Riehle MO, Johnstone HJH, Affrossman S, Curtis ASG. Polymer-demixed nanotopography: control of fibroblast spreading and proliferation. Tissue Eng 2002;8(6):1099–108.
[22] Dalby MJ, Yarwood SJ, Riehle MO, Johnstone HJH, Affrossman S, Curtis ASG. Increasing fibroblast response to materials using nanotopography: morphological and genetic measurements of cell response to 13-nm-high polymer demixed islands. Exp Cell Res 2002;276:1–9.